World Academy of Science, Engineering and Technology
International Journal of Aerospace and Mechanical Engineering
Vol:7, No:6, 2013

Numerical Analysis of the Influence of Tip Devices on the Power Coefficient of a VAWT

Federico Amato, Gabriele Bedon, Marco Raciti Castelli, Ernesto Benini

***Abstract*—The aerodynamic performances of vertical axis wind turbines are highly affected by tip vortexes. In the present work, different tip devices are considered and simulated against a baseline rotor configuration, with the aim of identifying the best tip architecture. Three different configurations are tested: winglets, an elliptic termination and an aerodynamic bulkhead. A comparative analysis on the most promising architectures is conducted, focusing also on blade torque evolution during a full revolution of the rotor blade. The most promising technology is concluded to be a well designed winglet.**

***Index Terms*—Darrieus Wind Turbine, Tip Devices, Tip Vortexes, Winglet, Elliptic Termination, Aerodynamic Bulkhead**

I. Introduction

All wind turbines operating by means of the lift force have blades created with aerodynamic airfoils. When these airfoils are invested by a fluid, because of the characteristic curvature of their sections, the flow particles on the suction side are faster than those on the pressure side. This generates a pressure difference and a consequent aerodynamic force on the profile itself.

In the hypothesis of an infinite blade span, the flux is the same on all the blade sections. This is an ideal situation that is not representative of reality, where the blade is characterized by a finite extension. In this case, the pressure difference between pressure and suction sides generates a flow along the blade extension: from the high pressure zone, the air flows around the blade tip to reach the lower pressure side, as exemplified in Figure 1. As a consequence of the pressure tendency on the suction side to equate the pressure value on the pressure side at the tip of the blade, the lifting force per unit length is lower in correspondence with the profile tips. The described phenomenon, of course, is related to the blade tip, being negligible in the central part of the blade.

The adoption of aerodynamic appendixes, finalized to reduce the above described phenomena, has recently become quite common in the aerospace industry. Three different solutions will be presented in this work: an aerodynamic bulkhead, a winglet and an elliptic termination. The first solution is very simple and easy to manufacture; winglets

Federico Amato completed his M.Sc. in Mechanical Engineering at the University of Padua, Via Venezia 1, 35131 Padua, Italy

Gabriele Bedon is a Ph.D. Student in Energy Engineering at the University of Padua, Via Venezia 1, 35131 Padua, Italy (e-mail: gabriele.bedon@dii.unipd.it).

Marco Raciti Castelli is a Research Associate at the Department of Industrial Engineering of the University of Padua, Via Venezia 1, 35131 Padua, Italy (e-mail: marco.raciticastelli@unipd.it).

Ernesto Benini is an Associate Professor at the Department of Industrial Engineering of the University of Padua, Via Venezia 1, 35131 Padua, Italy (e-mail: ernesto.benini@unipd.it).

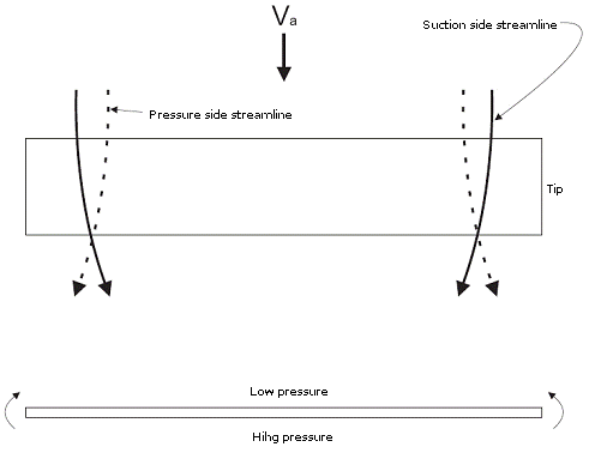

Fig. 1: Secondary fluxes from the pressure side to the suction one, due to a finite blade span.

are extensively studied in the aeronautic field [1] and some studies on their use on horizontal axis wind turbines are to be found in literature [2], [3]; the elliptic terminations ensure a reduction of tip effects, too, and have been adopted in the aeronautic field since the Second World War with the Spitfire fighter.

II. Downwash and Induced Drag

The tendency of the flow to wrap around the blade tip leads to a circulation that is moved downstream, creating the tip vortex shown in Figure 2.

Fig. 2: Tip vortex rolling up from a wingtip (from: [4])

This vortex downstream the profile generates a small component of the velocity towards the ground in the vicinity of the profile itself, called ”downwash”. This component, combined vectorially with the unperturbed velocity close to

the profile, causes a reduction in the geometrical angle of attack, as shown in Figure 3.

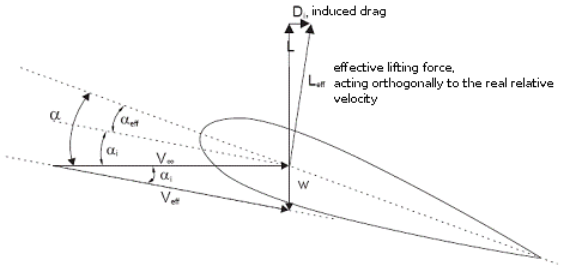

Fig. 3: Effect of the downwash on the local flux at the tip of a wing or a wind turbine blade

The angle between the chord direction and the freestream flux V_∞ is called "geometrical angle of attack", α. The local flux direction results inclined towards the ground with respect to the free stream flux of an angle α_i called "induced angle of attack". The deflection has therefore two effects on the flux that invest a generic profile section:

- the real angle of attack for the section is lower with respect to the geometrical one and is equal to the difference between the geometric angle of attack and the induced angle of attack, in formula:

$$\alpha_{\text{eff}} = \alpha - \alpha_i \tag{1}$$

- the vector which identifies the lifting force, being normal to the local direction of the relative velocity, is inclined, too, of an angle α_i. As a consequence, a local drag due to the deflection, called induced drag D_i, is generated.

III. The Case Study

The numerical analyses are conducted on the same rotor typology considered in the CFD validation conducted by Raciti Castelli et al. [5] and successively further investigated in [6], [7]. A full Computational Fluid Dynamics (CFD) campaign is performed in order to simulate the operation of a single-bladed Darrieus VAWT. Table I summarizes the main geometrical features of the investigated rotor geometry.

Rotor radius, R [mm]	515
Rotor blade number, N [-]	1
Blade profile	NACA 0021
Rotor blade chord, c [mm]	85.8

TABLE I: Main geometrical characteristics of the analyzed Darrieus rotor

An analytical code is coupled to a solid modeling software, capable of generating the desired rotor blade tip geometry, which is linked to a finite volume CFD code (the commercial software Ansys Fluent) for the calculation of rotor performance. CFD results are successively postprocessed using a second analytical code for the calculation of rotor main kinematic and dynamic characteristics. All the tested tip devices are added to the baseline blade profile, whose spanwise length is concordantly reduced, in order to maintain the same rotor swept area.

IV. Aerodynamic Bulkhead

A bulkhead is a very simple solution to increase the aerodynamic efficiency of a rotor blade. It consists of an enlargement of the blade tip section, for the purpose of forcing the flux to have bi-dimensional characteristics: as a matter of fact, the insertion of a bulkhead generates an obstacle to the secondary vortex that is generated at the blade tip, due to the pressure difference between suction and pressure sides.

The advantage of this solution is to be efficient for every azimuthal position of the blade profile along its revolution around rotor shaft. The analyzed bulkhead is in fact symmetric with respect to the blade profile and has therefore the same behaviour independently from the instantaneous pressure side (varying along with the azimuthal coordinate for a Darrieus VAWT).

Bulkheads are a very common solution in several engineering applications and are successfully adopted also in other technology fields, as can be seen from Figure 4.

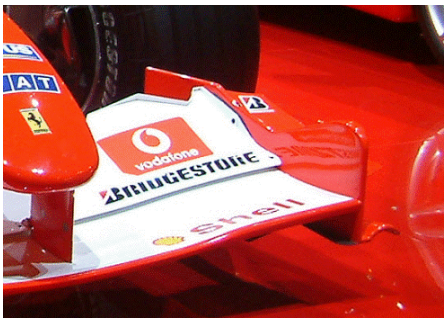

Fig. 4: Anterior aileron of a Formula 1 car

The tested model is realized with a bulkhead shape similar to the aerodynamic profile, characterized by an offset of around 10 mm, as reported in Figures 5, 6 and 7.

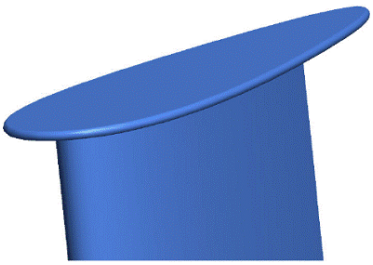

Fig. 5: General overview of the analyzed aerodynamic bulkhead

The application of an aerodynamic bulkhead presents several advantages:

- it is not expensive;
- it is a simple solution, the variables to be considered for its shape optimization are limited, mainly the offset and the tip shape;
- it does not require substantial changes in the turbine geometry;
- it can be applied even after the blade production and therefore it does not require changes in the production chain.

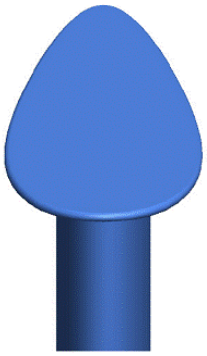

Fig. 6: Frontal view of the analyzed aerodynamic bulkhead

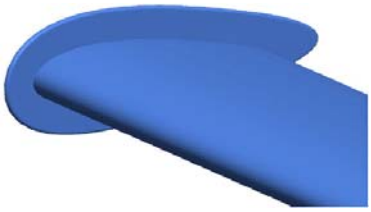

Fig. 7: Bottom view of the analyzed aerodynamic bulkhead

Among the disadvantages to be considered:

- an additional weight is introduced, even if limited, to the blade tip, leading to more bending moments due to the centrifugal force close to blade-spoke connection;
- it is not a good aesthetic solution.

V. Winglet

Winglets are tip devices that are inserted at the blade extreme sections in order to reduce tip vortexes and, consequently, to increase the aerodynamic efficiency of the blade. Their applications are mainly limited to the aeronautical field [8], both civil and military.

A. Geometry

The plan view of a winglet can be considered as the figure obtained by rotating it up to the main profile plan. For the proposed work, the geometry of the tested blade/winglet architectures is described by some characteristic parameters:

- Φ the cant angle, defined as the angle between the plan of the blade and the axis of the winglet;
- l_w the length of the winglet;
- b the span of the blade profile;
- s half-span of the blade profile;

The link between the winglet and the main profile can create a sharp edge or have a curvature to obtain the so-called blended-winglet, as shown in Figure 8.

In the present work, characterized by symmetrical airfoil sections (NACA 0021), the trace of the blade profile is coincident to its leading edge, as shown in Figure 9. It will be used as a geometrical reference for all the analyzed models, in order to calculate the rotor swept area, as shown in Figure 10.

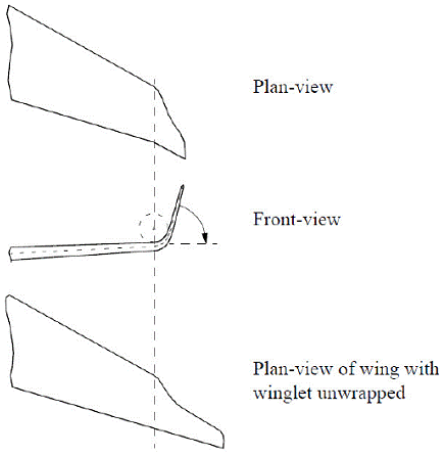

Fig. 8: Schematic views of a blended winglet

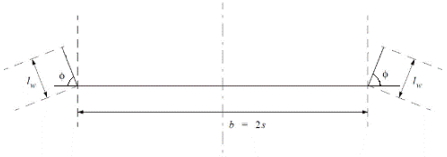

Fig. 9: Trace of the blade profile

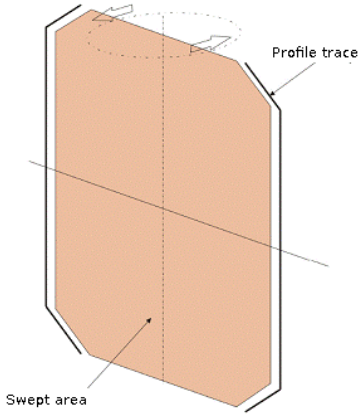

Fig. 10: Rotor swept area estimation

In their simplest realizations, winglets present a reduced chord length with respect to the main profile. They are generally not orthogonal to the blade plan, forming a cant angle comprised between 75° and 45°. In reviewing the literature, even more complex blade tip devices are registered, realized by means of two winglets, one pointing downward and the other upward. Such architectures are not included in the present work.

B. Analyzed Models

The first analyzed model consists of a classical winglet driven from literature [1]. It is characterized by a length of $l_w = 100$ mm and a cant angle of $\Phi = 60°$. For the connection to the blade profile, a ratio between winglet root chord and blade chord equal to 0.6 is considered, being commonly adopted in the aeronautical field. The tested winglet geometry

is shown in Figures 11, 12 and 13.

Fig. 11: Geometry of the first analyzed winglet

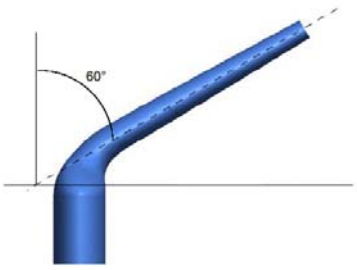

Fig. 12: Front view of the first analyzed winglet, with a cant angle of $\Phi = 60°$

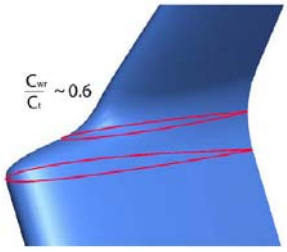

Fig. 13: Detail of the blade-winglet connection for the first analyzed winglet

Considering the same geometrical characteristics of the junction between the rotor blade and the winglet, a second model is created, characterized by some modifications. In particular, the cant angle is increased up to 90°.

Fig. 14: Geometry of the second analyzed winglet

Considering the high efficiency obtained for the model characterized by a cant angle of $\Phi = 90°$, a third model is developed, characterized by the same cant angle but with a length equal to $l_w = 150$ mm (50% more than the second model), as shown from Figure 15.

VI. Elliptic Tip Device

As can be drawn from Figure 16, in this last case the sections that characterize the blade tip are positioned in order to maintain a constant coordinate of the airfoil centre of pressure. This solution has the advantage of creating no aerodynamic bending moment in the plane of each external blade section, acting the aerodynamic force on the same point for each blade station, as shown in Figure 17.

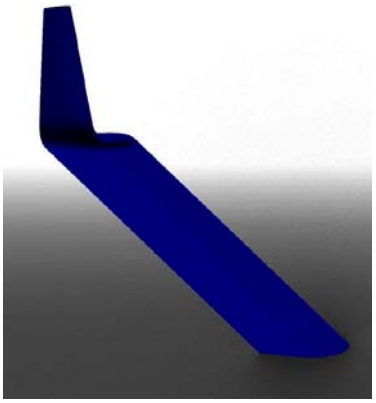

Fig. 15: Geometry of the third analyzed winglet

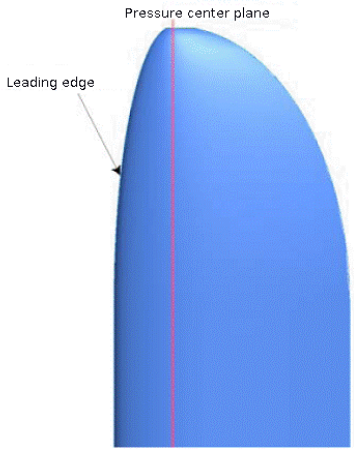

Fig. 16: Plan view of the rotor blade characterized by an elliptic tip

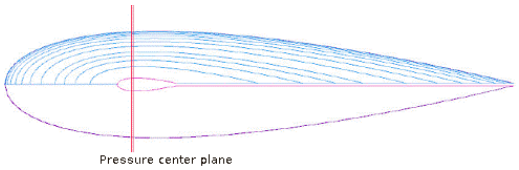

Fig. 17: Top view of the elliptic blade tip: the coordinate of the centre of pressure is kept constant along the whole blade span

The considered solution presents the advantage of weight reduction near the blade tip, with a consequent benefit regarding the bending moment generated by the centrifugal forces close to the blade-spoke connection.

VII. Spatial Domain Discretization

The proposed simulations are based on the wind tunnel measurements performed in Milan-Bovisa's low turbulence facility on a straight-bladed Darrieus rotor, made of three NACA 0021 airfoils characterized by a chord length of 85.8

mm, constructed of aluminum and carbon fibers. Before analyzing the models described in the previous section, a complete validation work has been conducted [5].

The analyzed models have kept the same main features of the validation model: a computational domain of rectangular shape has been chosen, having the same wind tunnel size. The boundary conditions consist of two lateral walls spaced 2000 mm apart from the wind tunnel centerline (the wind tunnel is 4000 mm wide and 3880 mm high).

As the aim of the present work is to reproduce the operation of a rotating machine, the use of moving sub-grids is mandatory. In particular, the discretization of the computational domain into macro-areas leads to two distinct sub-grids:

- an external zone characterized by a prismatic shape, with the same section of the testing room of the wind tunnel where the experimental measurements were conducted, with a cylindrical opening centered on the rotation axis of the turbine, that will be referred to as wind tunnel sub-grid;
- a cylindrical inner zone rotating with the same angular velocity of the turbine, that will be referred to as rotor sub-grid.

A. Wind Tunnel Sub-Grid

The main dimensions of the wind tunnel sub-grid are shown in Figure 18.

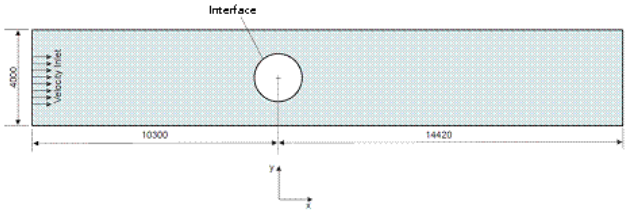

Fig. 18: Main geometrical characteristics of the wind tunnel sub-grid [mm]

Inlet and outlet boundary conditions are placed respectively 10 rotor diameters upwind and 14 rotor diameters downwind with respect to the rotor test section, allowing a full development of the wake. The cylindrical surface around the central opening is set as an interface, thus ensuring the continuity of the flow field.

B. Rotor Sub-Grid

The fluid area where the wind turbine rotation is simulated is characterized by a moving mesh, revolving at the same angular speed of the turbine, as shown in Figure 19. Its location coincides exactly with the cylindrical opening inside the wind tunnel sub-grid. The characteristic cell dimension on both sides of the interface is the same, in order to promote a rapid convergence [9].

An isotropic unstructured mesh is adopted for both the rotor sub-grid and the wind tunnel sub-grid, in order to obtain the same accuracy in the prediction of rotor performance during the revolution. As a final step, the mesh is fully converted into

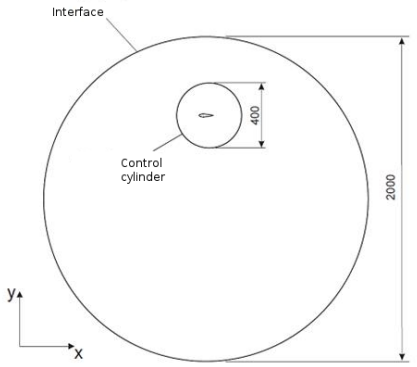

Fig. 19: Main geometrical characteristics of the rotor sub-grid [mm]

polyhedra. This option, applicable to unstructured meshes of tetrahedral type, presents the advantage of reducing the total number of grid elements, producing in the same time greater mesh regularity.

All the blade profiles inside the rotor sub-grid are enclosed in a control cylinder of 400 mm diameter, whose aim is to allow a precise dimensional control of the grid elements in the area close to the rotor blade, by adopting a first size function operating from the blade profile to the control cylinder itself and a second size function operating from the control cylinder to the whole rotor sub-grid volume, ending with grid elements of the same size of the corresponding wind tunnel sub-grid cells. An interior boundary condition is adopted for the borders of the control cylinder, thus ensuring the continuity of the cells on both sides of the grid.

For further details about the validation of the numerical code, see [5].

VIII. Bulkhead Meshing

Figures 20 and 21 show some views of the unstructured mesh adopted for the bulkhead. As can be seen, the adoption of a rounded corner (1 mm radius for a global thickness of 2 mm for the bulkhead) imposes a reduction of the characteristic cell size (0.7 mm), in order to correctly reproduce the analyzed geometry.

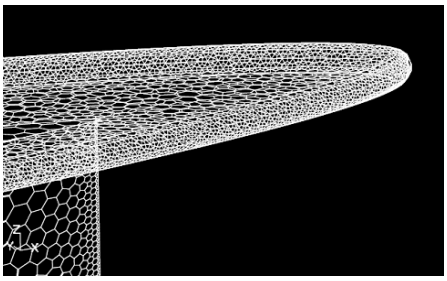

Fig. 20: Aerodynamic bulkhead, general overview of the unstructured mesh

Figure 22 shows the size functions which are adopted in order to link the reduced cell size in correspondence of the rounded corner to the cell size on the blade profile, while Figure 23 shows a top view of the aerodynamic bulkhead, where the different cell size between tip and central elements can be appreciated.

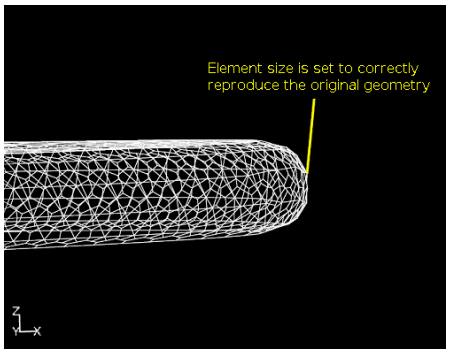

Fig. 21: Aerodynamic bulkhead, reduction of the characteristic cell size due to the rounded corner

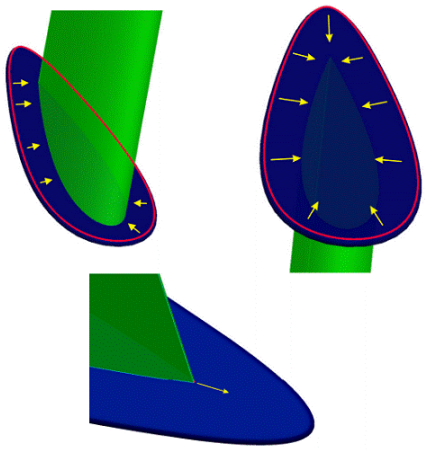

Fig. 22: Size functions on the bulkhead

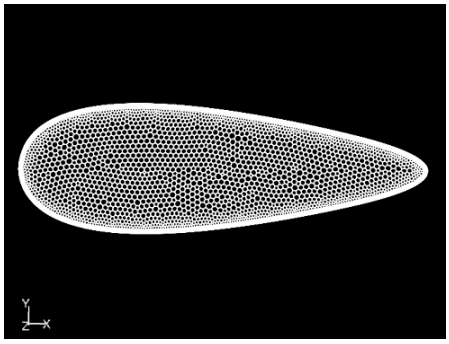

Fig. 23: Aerodynamic bulkhead, top view of the main surface

IX. Winglet and Elliptic Tip Meshing

Both winglet and elliptic tip meshing are characterized by the same size functions adopted for the blade profile, as shown in Figure 24.

X. Temporal Discretization and Turbulence Model Selection

As a global convergence criterion, each simulation is run until the instantaneous torque values show a deviation of less than 1% with respect to the corresponding values of the previous revolution. The residual convergence criterion for each physical time step is set to 10^{-5}.

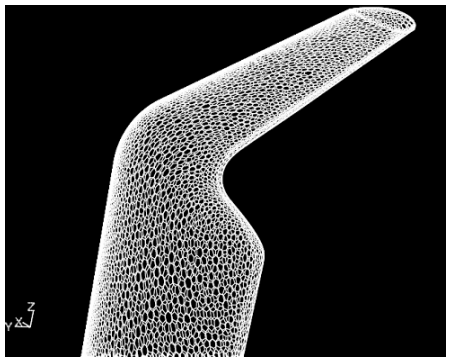

Fig. 24: Winglet unstructured mesh, created adopting the same cell size characteristics of the blade profile

The adopted meshing strategy aims at obtaining $y^+ = 30$ over the whole blade span. The selected turbulence model is the well known $k-\omega$ SST, as suggested by Raciti Castelli et al. [5], [6], [7]. This is considered as a reference model on the basis of a literature review, in particular because it provides a better analysis of the flow separation which occurs from rotor blades.

XI. Results and Discussion

Figure 25 shows the evolution of the rotor power coefficient, in formula:

$$C_P = P/(0.5\rho A V_\infty^3) \tag{2}$$

as a function of the tip speed ratio, defined as:

$$\lambda = \omega R \tag{3}$$

for all the tested tip configurations.

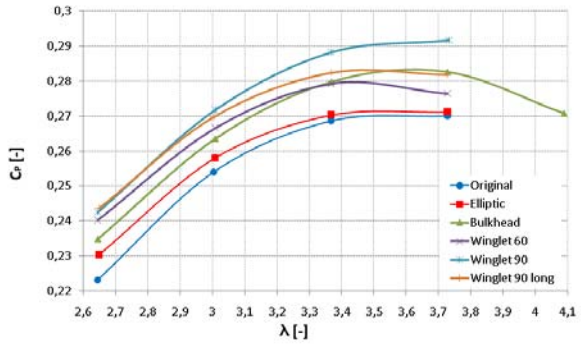

Fig. 25: Power curves for all the analyzed tip configurations

The optimal values of the power coefficient for all the tested tip architectures are reported in Table II.

The elliptic tip and the winglet characterized by a cant angle of 60° present a lower efficiency with respect to the rotor without any tip device, while the adoption of the aerodynamic bulkhead leads to an increase in rotor performance. Considering the winglets characterized by a cant angle equal to 90°, both the configurations determine an increase in rotor performance, with a higher value for the

Model	*Cp [-]*	λ *[-]*	*n [rpm]*
Baseline	0.280	3.4	573
Bulkhead	0.283	3.5	584
Elliptic	0.275	3.6	596
Winglet $\Phi = 60°$	0.273	3.6	595
Winglet $\Phi = 90°$	0.292	3.6	606
Winglet $\Phi = 90°$ long	0.283	3.6	602

TABLE II: Maximum power coefficient as a function of the rotational speed for all the tested tip configurations

shorter winglet. The physics of these last two solutions is investigated more deeply through a comparison between the two torque contributions (viscous and pressure) provided to the rotor shaft, as shown in Figures 26, 27 and 28.

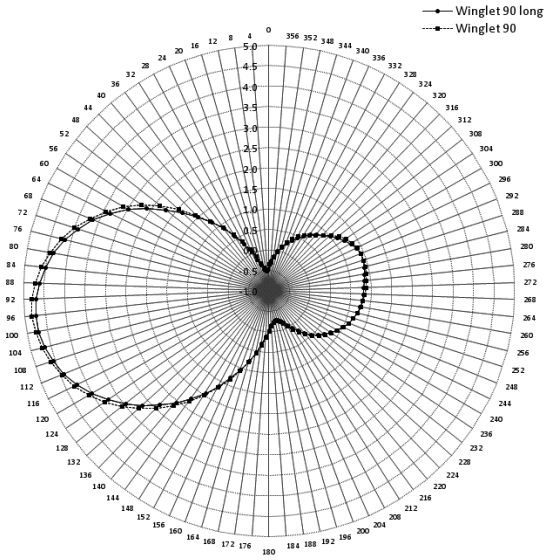

Fig. 26: Torque due to the viscous forces as a function of the azimuthal position for the two rotors characterized by a winglet with cant angle of 90°

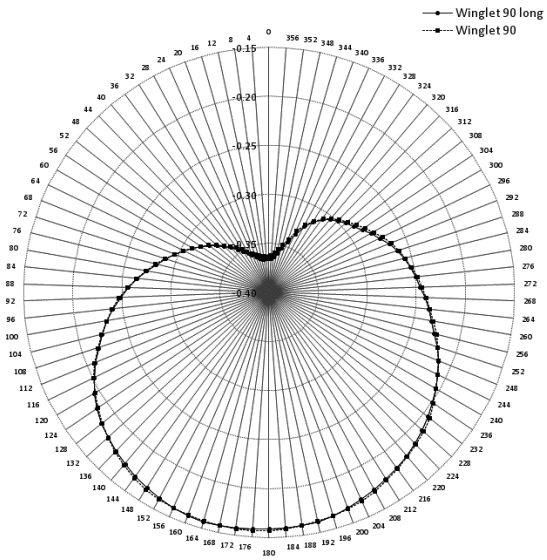

Fig. 27: Torque due to the pressure forces as a function of the azimuthal position for the two rotors characterized by a winglet with cant angle of 90°

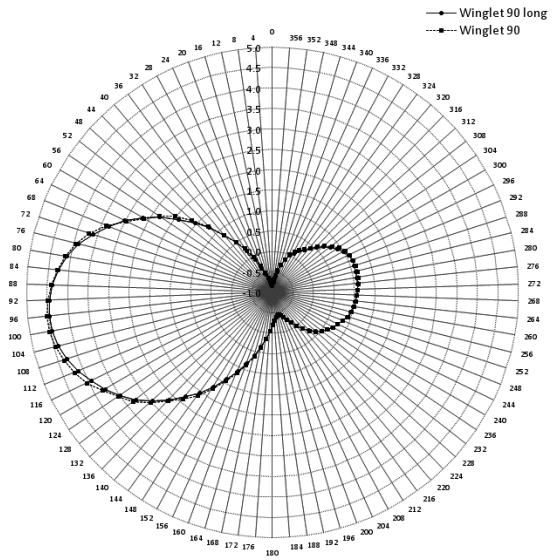

Fig. 28: Total torque as a function of the azimuthal position for the two rotors characterized by a winglet with cant angle of 90°

The lowest increase in rotor performances obtained by the solution with the longest winglet is due to the increase in the viscous torque and a contemporary decrease in the pressure torque on the profile, as highlighted from Table III.

Pressure torque	-2.504%
Viscous torque	+0.373%
Total torque	-3.089%

TABLE III: Percentage variations of the torque components at the rotor shaft for the long winglet architecture with respect to the short one

A comparative analysis on the performances of the different solutions is also conducted for the two main portions of rotor blade revolution (upwind and downwind). As can be clearly seen, during the downwind revolution, the blade is influenced by the aerodynamic effect of its own passage in the upwind section. The results are shown for a rotational speed of 560 rpm in Table IV and for 620 rpm in Table V.

Model	$T_{\mathbf{up}}$ **[Nm]**	**Incr. [%]**	$T_{\mathbf{dw}}$ **[Nm]**	**Incr. [%]**
Baseline	2.050	0.00	0.553	0.00
Bulkhead	2.080	+1.46	0.551	-0.36
Elliptic	1.960	-4.39	0.558	+0.90
Winglet $\Phi = 60°$	1.970	-3.90	0.558	+0.90
Winglet $\Phi = 90°$ long	2.040	-0.49	0.567	+2.53

TABLE IV: Average torques for the different tip solutions during both the upwind and the downwind passages, 560 rpm

Model	$T_{\mathbf{up}}$ **[Nm]**	**Incr. [%]**	$T_{\mathbf{dw}}$ **[Nm]**	**Incr. [%]**
Baseline	2.050	0.00	0.346	0.00
Bulkhead	2.020	+2.02	0.357	+3.18
Elliptic	1.910	-3.54	0.378	+9.25
Winglet $\Phi = 60°$	1.940	-2.02	0.356	+2.89
Winglet $\Phi = 90°$	2.070	+4.55	0.387	+11.85
Winglet $\Phi = 90°$ long	2.006	+1.31	0.374	+8.09

TABLE V: Average torques for the different tip solutions during both the upwind and the downwind passages, 620 rpm

XII. Conclusions

Three different technical solutions (an aerodynamic bulkhead, a winglet and an elliptic tip device) finalized to the reduction of the tip effects are analyzed on a small straight-bladed Darrieus vertical axis wind turbine. The adoption of the aerodynamic bulkhead increases the aerodynamic performance of the original model strongly, while the use of the winglet needs to be carefully investigated: if correctly realized, it produces a marked increase in rotor performance but, in a wrong realization, leads to lower rotor performances with respect to the original model without any tip device. In particular, a correct design determines an increase in rotor performance of more than 10% in the downwind section, where the flow field is characterized by vortexes generated by the blade itself during the upwind passage. The application of an elliptic extension determines a reduction in rotor performance, but the presented analysis has been limited to a single model. Further work should be done, in order to investigate the efficiency of an optimized elliptic tip on overall rotor performances.

Nomenclature

$A\ [m^2]$	Rotor swept area
$b\ [mm]$	Blade profile span
$c\ [mm]$	Rotor blade chord
$C_P\ [-]$	Rotor power coefficient
$D_i\ [N]$	Induced drag
$l_w\ [mm]$	Winglet length
$n\ [rpm]$	Rotor angular velocity
$N\ [-]$	Rotor blade number
$R\ [mm]$	Rotor radius
$s\ [mm]$	Blade profile semi-span
$T_{dw}\ [Nm]$	Average torque produced during the downwind portion of rotor blade revolution
$T_{up}\ [Nm]$	Average torque produced during the upwind portion of rotor blade revolution
$V_\infty\ [m/s]$	Freestream wind speed
$\alpha\ [^\circ]$	Geometrical angle of attack
$\alpha_{eff}\ [^\circ]$	Real angle of attack
$\alpha_i\ [^\circ]$	Induced angle of attack
$\lambda\ [-]$	Tip speed ratio
$\Phi\ [^\circ]$	Cant angle
$\rho\ [kg/m^3]$	Air density
$\omega\ [rad/s]$	Rotor angular velocity

References

[1] M. Freestone, "Aerodynamic Principles of Winglets," *Engineering Science Data Unit*, 1998.

[2] J. Johansen and N. Sø rensen, "Aerodynamic investigation of winglets on wind turbine blades using CFD," *RisøNational Laboratory Report Risø-R-1543(EN)*, 2006.

[3] M. Gaunaa and J. Johansen, "Determination of the maximum aerodynamic efficiency of wind turbine rotors with winglets," *Journal of Physics: Conference Series*, vol. 75, p. 012006, 2007.

[4] Wikipedia, "http://en.wikipedia.org/wiki/File:Airplane_vortex_edit.jpg," *accessed on May 2013*.

[5] M. Raciti Castelli, G. Ardizzon, L. Battisti, E. Benini, and G. Pavesi, "Modeling Strategy and Numerical Validation for a Darrieus Vertical Axis Micro-Wind Turbine," *Proceedings of the ASME 2010 International Mechanical Engineering Congress & Exposition IMECE2010-39548*, 2010.

[6] M. Raciti Castelli and E. Benini, "Effect of blade inclination angle on a Darrieus wind turbine," *Journal of Turbomachinery*, vol. 134, pp. 031016–1–10, 2012.

[7] M. Raciti Castelli, A. Dal Monte, M. Quaresimin, and E. Benini, "Numerical evaluation of aerodynamic and inertial contributions to Darrieus wind turbine blade deformation," *Renewable Energy*, vol. 51, pp. 101–112, 2013.

[8] R. Nangia, M. Palmer, and R. Doe, "Aerodynamic design studies of conventional & unconventional wings with winglets," *24 th AIAA Applied Aerodynamics Conference*, 2006.

[9] Fluent Inc., "Fluent Users Manual," pp. 52, 54, 59, 71, 143.